

Plasmonic band gap structures for surface-enhanced Raman scattering

Askin Kocabas,¹ Gulay Ertas,² S. Seckin Senlik¹
and Atilla Aydinli^{1,*}

¹ Department of Physics, Bilkent University, 06800, Ankara, Turkey

² Department of Chemistry, Bilkent University, 06800, Ankara, Turkey

*Corresponding author: aydinli@fen.bilkent.edu.tr

Abstract: Surface-enhanced Raman Scattering (SERS) of rhodamine 6G (R6G) adsorbed on biharmonic metallic grating structures was studied. Biharmonic metallic gratings include two different grating components, one acting as a coupler to excite surface plasmon polaritons (SPP), and the other forming a plasmonic band gap for the propagating SPPs. In the vicinity of the band edges, localized surface plasmons are formed. These localized plasmons strongly enhance the scattering efficiency of the Raman signal emitted on the metallic grating surfaces. It was shown that reproducible Raman scattering enhancement factors of over 10^5 can be achieved by fabricating biharmonic SERS templates using soft nano-imprint technique. We have shown that the SERS activities from these templates are tunable as a function of plasmonic resonance conditions. Similar enhancement factors were also measured for directional emission of photoluminescence. At the wavelengths of the plasmonic absorption peak, directional enhancement by a factor of 30 was deduced for photoluminescence measurements.

©2008 Optical Society of America

OCIS codes: (240.6680) Surface plasmon; (350.2770) Gratings; (300.6450) Raman spectroscopy.

References and Links

1. G. C. Schatz, M. A. Young, and R. P. Van Duyne, "Electromagnetic mechanism of SERS," in *Surface-Enhanced Raman Scattering: Physics and Applications* (2006), pp. 19-45.
2. E. J. Bjerneld, F. Svedberg, P. Johansson, and M. Kall, "Direct observation of heterogeneous photochemistry on aggregated Ag nanocrystals using Raman spectroscopy: The case of photoinduced degradation of aromatic amino acids," *J. Phys. Chem. A* **108**, 4187-4193 (2004).
3. K. A. Bosnick, J. Jiang, and L. E. Brus, "Fluctuations and local symmetry in single-molecule rhodamine 6G Raman scattering on silver nanocrystal aggregates," *J. Phys. Chem. B* **106**, 8096-8099 (2002).
4. A. Campion and P. Kambhampati, "Surface-enhanced Raman scattering," *Chem. Soc. Rev* **27**, 241-250 (1998).
5. W. E. Doering and S. M. Nie, "Single-molecule and single-nanoparticle SERS: Examining the roles of surface active sites and chemical enhancement," *J. Phys. Chem. B* **106**, 311-317 (2002).
6. M. Kall, H. X. Xu, and P. Johansson, "Field enhancement and molecular response in surface-enhanced Raman scattering and fluorescence spectroscopy," *J. Raman Spectrosc.* **36**, 510-514 (2005).
7. A. M. Michaels, M. Nirmal, and L. E. Brus, "Surface enhanced Raman spectroscopy of individual rhodamine 6G molecules on large Ag nanocrystals," *J. Am. Chem. Soc.* **121**, 9932-9939 (1999).
8. M. Moskovits, "Surface-Enhanced Spectroscopy," *Rev. Mod. Phys.* **57**, 783-826 (1985).
9. M. Kerker, "Electromagnetic model for surface-enhanced Raman scattering (SERS) on metal colloids," *Acc. Chem. Res.* **17**, 271-277 (1984).
10. M. Kerker, O. Siiman, L. A. Bumm, and D. S. Wang, "Surface enhanced Raman scattering (SERS) of citrate ion adsorbed on colloidal silver," *Appl. Opt.* **19**, 3253 (1980).
11. K. Kneipp, Y. Wang, H. Kneipp, L. T. Perelman, I. Itzkan, R. Dasari, and M. S. Feld, "Single molecule detection using surface-enhanced Raman scattering (SERS)," *Phys. Rev. Lett.* **78**, 1667-1670 (1997).
12. A. D. McFarland, M. A. Young, J. A. Dieringer, and R. P. Van Duyne, "Wavelength-scanned surface-enhanced Raman excitation spectroscopy," *J. Phys. Chem. B* **109**, 11279-11285 (2005).
13. F. J. GarciaVidal and J. B. Pendry, "Collective theory for surface enhanced Raman scattering," *Phys. Rev. Lett.* **77**, 1163-1166 (1996).

14. S. M. Nie and S. R. Emery, "Probing single molecules and single nanoparticles by surface-enhanced Raman scattering," *Science* **275**, 1102-1106 (1997).
15. H. H. Wang, C. Y. Liu, S. B. Wu, N. W. Liu, C. Y. Peng, T. H. Chan, C. F. Hsu, J. K. Wang, and Y. L. Wang, "Highly Raman-enhancing substrates based on silver nanoparticle arrays with tunable sub-10 nm gaps," *Adv. Mater.* **18**, 491 (2006).
16. K. Kneipp, G. R. Harrison, S. R. Emory, and S. M. Nie, "Single-molecule Raman spectroscopy - Fact or fiction?," *Chimia* **53**, 35-37 (1999).
17. K. Kneipp, H. Kneipp, I. Itzkan, R. R. Dasari, and M. S. Feld, "Ultrasensitive chemical analysis by Raman spectroscopy," *Chem. Rev.* **99**, 2957 (1999).
18. J. J. Baumberg, T. A. Kelf, Y. Sugawara, S. Cintra, M. E. Abdelsalam, P. N. Bartlett, and A. E. Russell, "Angle-resolved surface-enhanced Raman scattering on metallic nanostructured plasmonic crystals," *Nano Lett.* **5**, 2262-2267 (2005).
19. N. M. B. Perney, J. J. Baumberg, M. E. Zoorob, M. D. B. Charlton, S. Mahnkopf, and C. M. Netti, "Tuning localized plasmons in nanostructured substrates for surface-enhanced Raman scattering," *Opt. Express* **14**, 847-857 (2006).
20. N. M. B. Perney, F. J. G. de Abajo, J. J. Baumberg, A. Tang, M. C. Netti, M. D. B. Charlton, and M. E. Zoorob, "Tuning localized plasmon cavities for optimized surface-enhanced Raman scattering," *Phys. Rev. B* **76**, 035426 (2007).
21. I. Baltog, N. Primeau, R. Reinisch, and J. L. Coutaz, "Surface-Enhanced Raman-Scattering on Silver Grating - Optimized Antennalike Gain of the Stokes Signal of 10(4)," *Appl. Phys. Lett.* **66**, 1187-1189 (1995).
22. M. Kahl, and E. Voges, "Analysis of plasmon resonance and surface-enhanced Raman scattering on periodic silver structures," *Phys. Rev. B* **61**, 14078-14088 (2000).
23. W. Knoll, M. R. Philpott, J. D. Swalen, and A. Girlando, "Surface-Plasmon Enhanced Raman-Spectra of Monolayer Assemblies," *J. Chem. Phys.* **77**, 2254-2259 (1982).
24. A. Nemetz, U. Fernandez, and W. Knoll, "Surface-Plasmon Field-Enhanced Raman-Spectroscopy with Double Gratings," *J. Appl. Phys.* **75**, 1582-1585 (1994).
25. A. C. R. Pipino, R. P. VanDuyne, and G. C. Schatz, "Surface-enhanced second-harmonic diffraction: Experimental investigation of selective enhancement," *Phys. Rev. B* **53**, 4162-4169 (1996).
26. A. Kocabas, S. S. Senlik, and A. Aydinli, "Plasmonic band gap cavities on biharmonic Gratings," *Phys. Rev. B* **77**, 195130 (2008).
27. W. L. Barnes, T. W. Preist, S. C. Kitson, and J. R. Sambles, "Physical origin of photonic energy gaps in the propagation of surface plasmons on gratings," *Phys. Rev. B* **54**, 6227-6244 (1996).
28. P. Hildebrandt and M. Stockburger, "Surface-Enhanced resonance Raman-Spectroscopy of Rhodamine-6G adsorbed on colloidal silver," *J. Phys. Chem.* **88**, 5935-5944 (1984).
29. Y. Chen, K. Munechika, and D. S. Ginger, "Dependence of fluorescence intensity on the spectral overlap between fluorophores and plasmon resonant single silver nanoparticles," *Nano Lett.* **7**, 690-696 (2007).
30. N. F. Chiu, C. Yu, S. Y. Nien, J. H. Lee, C. H. Kuan, K. C. Wu, C. K. Lee, and C. W. Lin, "Enhancement and tunability of active plasmonic by multilayer grating coupled emission," *Opt. Express* **15**, 11608-11615 (2007).
31. E. Takeda, M. Fujii, T. Nakamura, Y. Mochizuki, and S. Hayashi, "Enhancement of photoluminescence from excitons in silicon nanocrystals via coupling to surface plasmon polaritons," *J. Appl. Phys.* **102**, 023506 (2007).
32. J. Y. Wang, Y. W. Kiang, and C. C. Yang, "Emission enhancement behaviors in the coupling between surface plasmon polariton on a one-dimensional metallic grating and a light emitter," *Appl. Phys. Lett.* **91**, 233104 (2007).
33. Y. Wang and Z. P. Zhou, "Strong enhancement of erbium ion emission by a metallic double grating," *Appl. Phys. Lett.* **89**, 253122 (2006).

1. Introduction

Raman spectroscopy is a crucial tool in the analysis of vibrational bonds which reveal the details of the molecular structure. Despite its importance, extremely low cross section of Raman scattering ($10\text{-}30\text{ cm}^2$ per molecule) [1] limits its applications in chemical and biological sensing. However, in the vicinity of the noble metal nanoparticles (such as Ag and Au), physical mechanism of the Raman scattering is dramatically altered which results in considerable signal enhancement. This phenomenon is known as Surface Enhanced Raman Scattering (SERS) and the physics behind this enhancement have been extensively studied. The mechanism and applications of SERS have been reported on several review and feature articles [2-6]. It has been shown that localized and propagating plasmons play an essential role in this process. In particular, metallic nanoparticles can absorb light in visible wavelength range and support localized plasmon modes. When the large electric fields generated by these localized modes are at the incoming resonance wavelengths, they lead to large enhancements in the electric field intensity. It should be noted that enhanced Raman signal roughly scales

with (E_s^4) [7, 8] where E_s is the local electric field. This mechanism does not require chemisorption and in general predicts equal enhancements for all molecules with maximum enhancement factors of 10^6 - 10^7 [4, 8-11]. In addition, nanoparticles can also increase the out of plane scattering of the Raman signal emitted on their surface at the outgoing resonance wavelengths [1]. It has been previously shown that most favorable condition for SERS is observed when plasmonic resonance absorption lies between the exciting laser and Raman emission wavelengths [12]. With the help of the metallic nanoparticles, the enhancement factors up to 10^{15} allowing single molecule detection, have been reported [11, 13-17]. Efforts to understand and develop SERS as an analytical tool are dependent on methods for fabricating templates with stable and reproducibly high activities. Typical SERS substrates, textured metallic surfaces such as spherical shapes [18] and pyramidal type voids [19, 20] allow engineering the plasmonic modes to optimize reproducible SERS enhancement. These kinds of structures can support localized plasmonic modes and also localize the propagating surface plasmon inside the voids. On the other hand, rather than voids, metallic grating surfaces can also act as SERS templates [21-24]. Raman signal emitted at the near field of the metallic grating couples to the SPP and is re-radiated into the photon at a specific direction determined by both the wavelength of radiation and the periodicity of the grating. When a Raman active material is deposited on a flat surface, Stokes radiation is emitted into a solid angle of 2π sr. However, on a metal grating surface, Stokes radiation is confined into a much smaller solid angle and results in an enhancement in the measured Raman signal [21]. These types of templates show relatively low enhancement factors (10^4) [21] and enhanced Stokes wavelengths depend on the collection angle as well [23].

In this work, we demonstrate that biharmonic metallic grating structures can be used as SERS substrates. Previously, biharmonic grating structures have been used to enhance second harmonic generation [25] and to form plasmonic band gap cavities [26]. Biharmonic surface is made up of a grating with two harmonic components. Higher periodicity couples the incident light into the SPPs while the second shorter grating component forms a plasmonic band gap. Due to the flat dispersion at the vicinity of the band edges, plasmonic density of states is perturbed and effective coupling of emitted signal into the SPP are achieved. We demonstrate the SPP coupled enhancement of PL and SERS signals. Soft nanoimprint technique is used as a replication tool allowing the fabrication of SERS templates reproducibly.

2. Fabrication of biharmonic gratings

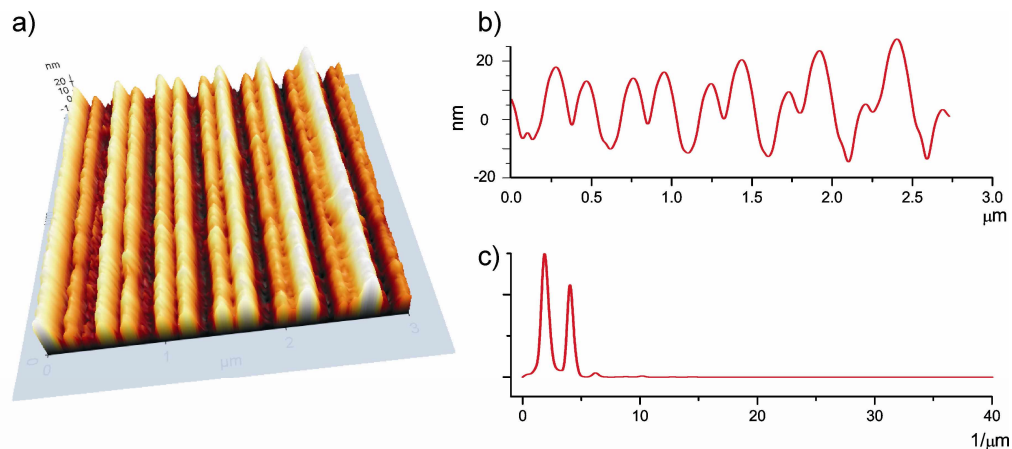


Fig. 1.(a) 2D AFM image of biharmonic metallic surface includes $\Lambda_1=500$ nm and $\Lambda_2=250$ nm gratings. First periodicity is designed to excite the SPP's. Second one generates backscattering for propagating SPP's and opens up a photonic band gap. (b) Line profile of AFM image. (c) Power spectrum of AFM image indicating two different harmonic components.

Shown in Fig. 1(a) is the AFM image of fabricated biharmonic template. Gratings with two different periods were successively recorded on a photosensitive polymer (AZ1505) by holographic double exposure technique. Figure 1(b) shows line profile of the biharmonic grating, including two different grating components with periodicities of $\Lambda_1=500$ nm and $\Lambda_2=250$ nm. As seen in Fig. 1(c), power spectrum clearly shows these two different superimposed grating components. Once developed, the structure was transferred onto the photo-curable epoxy by soft nano-imprint technique. The replication procedure of the template structure to the polymeric surface is shown schematically in Fig. 2. In this procedure, biharmonic master grating template was prepared using interference lithography (Fig. 2(a)), which is used to make the elastomeric stamp. Liquid PDMS (Sylgard 184, Dow Corning) was poured on the master grating (Fig. 2(b)) and cured at 75 °C for 2 h. After the curing procedure, elastomeric stamp was peeled off from the master grating (Fig. 2(c)) and placed on the pre-polymer (OG 146, Epoxy Technology) coated wafer (Fig. 2(d)). Pre-polymer was then cured using UV light exposure (Fig. 2(e)). Finally, the elastomeric stamp was mechanically removed from the wafer (Fig. 2(f)). The photocurable epoxy is chemically inert for the latter processes. 55 nm-thick gold (Au) films were evaporated on cured epoxy to form a metallic periodic structure.

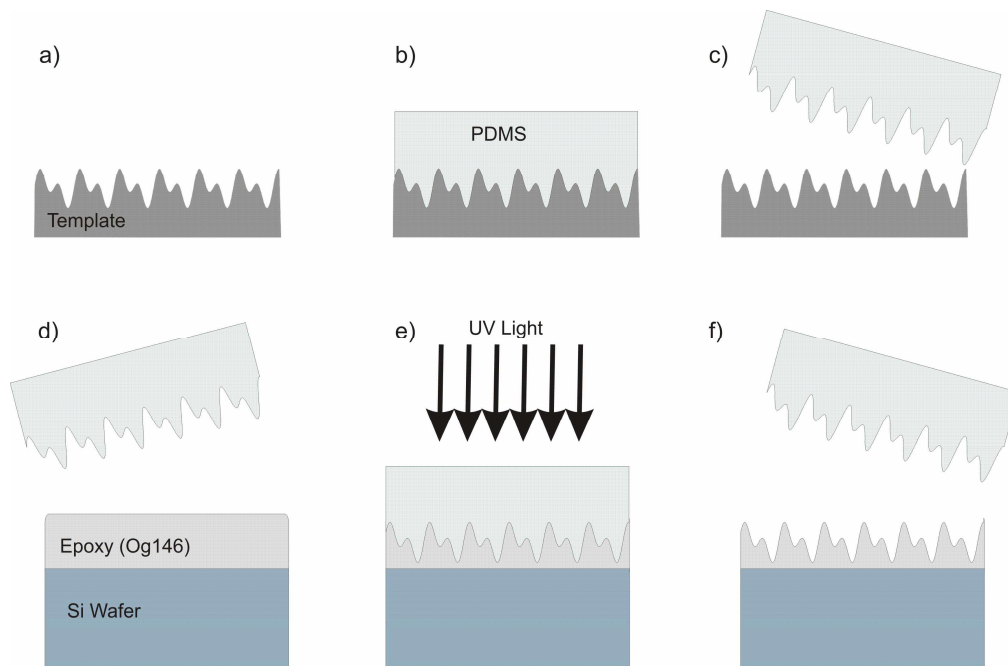


Fig. 2. Schematic diagram for replication and transfer of the grating structure onto the polymeric surface using the elastomeric stamp (PDMS); (a) Biharmonic master grating template was prepared using interference lithography, (b) the template was prepared by pouring liquid PDMS on the master grating and then cured at 75 °C for 2 h. (c) After the curing procedure, the elastomeric stamp was peeled off from the master grating, (d) and then, placed on the pre-polymer (OG146) coated wafer (e) where the pre-polymer was exposed to UV light. (f) Finally, the elastomeric stamp was mechanically removed from the wafer.

Optical reflectivity measurements were carried out using a spectroscopic ellipsometer (WVASE32) to investigate the plasmonic excitation on the biharmonic metallic surface. Figure 3 shows the normal incidence reflection spectra of as prepared templates for different metallic (Ag and Au) layers. Ag metal shows superior optical response than the Au metal in the visible wavelength range. As seen in Fig. 3, additional absorption minima occur in TM polarized reflection spectra (electric fields perpendicular to the grating groves). Two different minima correspond to excitation of SPPs at the band edges of the photonic band gap region.

Uniform $\Lambda_1=500$ nm grating component creates coupling between the incoming light and the SPPs propagating in both forward and backward directions. However, superimposed second grating ($\Lambda_2=250$ nm) creates back scattering for SPPs. Interfering SPPs form a standing wave having two different localization profiles [27]. As shown in Fig. 3(c) and Fig. 3(d), are the finite difference time domain (FDTD) simulation results and show electric field distribution for these localizations. λ^- localizes on the troughs, while λ^+ localizes on the peaks of the periodic structure [27]. In these simulations, Drude model was used to calculate the dielectric response of the metal. In the visible wavelength range, Drude model cannot fully explain the exact field enhancement. However, localized field profiles can be clearly demonstrated. Similarly, reflectivity measurements were also made for Au deposited biharmonic templates. Au metal is highly resistive towards chemical oxidation when compared with Ag metal, therefore, Au coated biharmonic structures were used as SERS substrates throughout this study. As seen in Fig. 3(b), a similar reflectivity spectrum was measured for Au metal. The reason for decrease in reflectivity for both metals below 500 nm is diffraction from the 500 nm grating periodicity. Above 500 nm wavelength scale, diffraction becomes evanescent. Figure 4 shows the experimental dispersion diagrams for biharmonic and uniform grating structures. In biharmonic gratings band gap opens up in the dispersion diagram and flattens the bands around the band edges. The periodicity of the uniform grating is 665 nm. Gratings were fabricated on transparent glass substrates and dispersion diagrams were constructed by scanning the incidence angle and measuring the transmission spectrum. Plasmonic excitation creates an enhancement in transmission. The dispersion diagrams are constructed by tracking the enhancement in transmission as a function of angle.

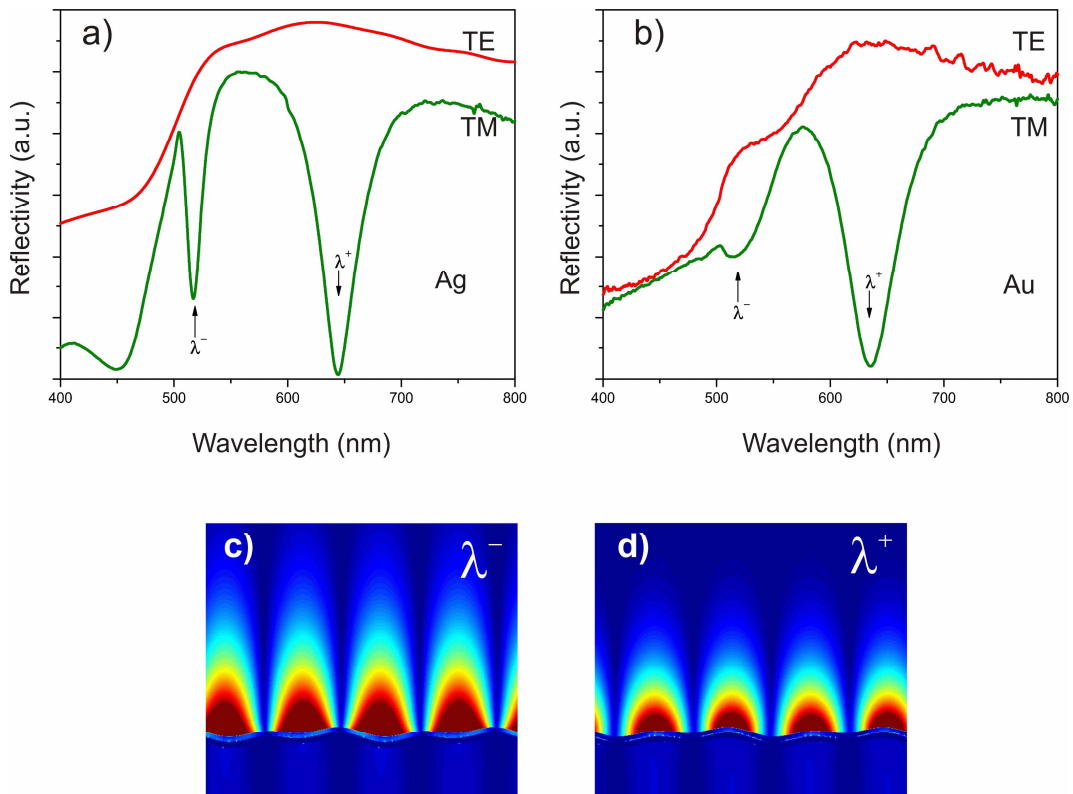


Fig. 3. Reflectivity spectra for biharmonic gratings coated with metallic film a) Ag and b) Au. Simulation results for electric field distributions on a biharmonic metallic grating structure illuminated with the wavelength of c) λ^- and d) λ^+ , respectively. λ^- localizes on the troughs, while λ^+ localizes on the peaks of the periodic structure.

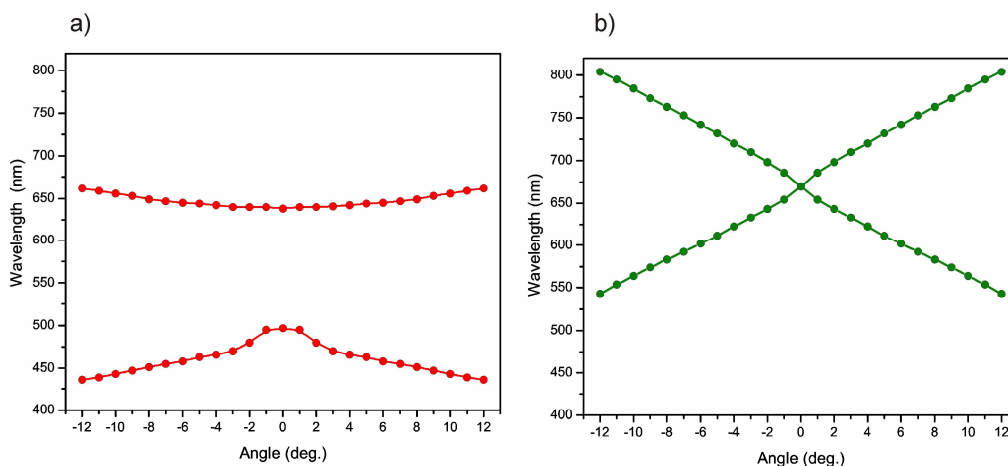


Fig. 4. Experimental dispersion diagrams for a) biharmonic and b) uniform grating structures.

3. Surface enhanced Raman scattering

Raman spectra were obtained with a Jobin Yvon LABRAM Raman Spectrometer equipped with a He-Ne laser which gave excitation line at 632.81 nm. The incident power was 20 mW and the laser beam was focused by a 10x objective lens. The scattered radiation was collected by the same objective lens and sent through a Raman notch filter to a Peltier cooled CCD detector. 10 μl of 10^{-6} M Rodamine 6G (see the inset of Fig. 5) solutions were drop-coated onto the template and were then allowed to dry. The SPP absorption spectrum at normal incidence and the SERS spectrum of R6G molecule are shown as green and red curves in Fig. 5, respectively. Raman bands at 616, 777, 1191 cm^{-1} associate with C-C-C ring in-plane, out of plane bending and C-C stretching vibrations, respectively, as well as bands at 1364, 1512 and 1653 cm^{-1} which are usually assigned to aromatic C-C stretching vibrations of R6G molecule [28]. After the molecular deposition, effective index of the SPP environment slightly changes. This makes plasmonic absorption shift towards the longer wavelengths by about 10 nm. After subtracting the background, empirical signal enhancement factors were determined using peak integrated ratios of the surface enhanced Raman vibration to the corresponding unenhanced signal from 55 nm thick Au metal surface coated on Si surface. Enhancement factor of 10^5 which is 10 times better than that of uniform grating surfaces [21] was measured.

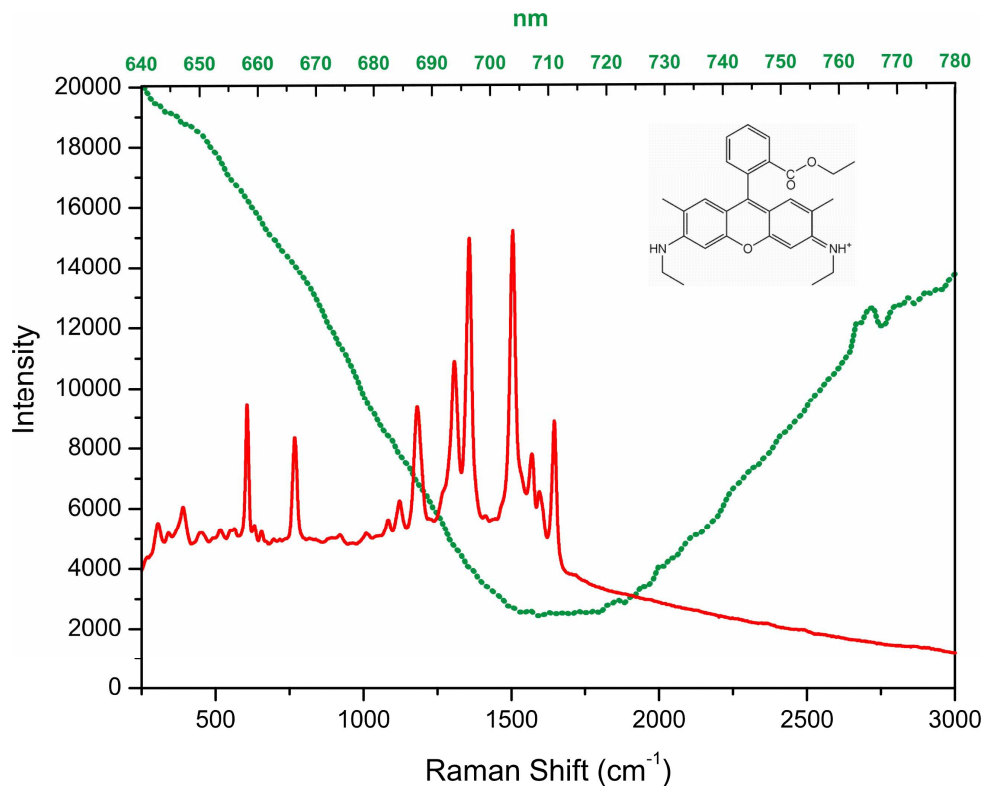


Fig. 5. SERS spectrum of 10^{-6} M R6G spectrum taken from the biharmonic surface coated with Au metal with an integration time of 1s (Red curve). Green curve represents the normal incidence reflectivity of biharmonic plasmonic template. Inset shows the molecular structure of R6G molecule.

Resonance absorption wavelength dependence of SERS signal can provide a key insight into the mechanism leading to SERS enhancement. We observed that grating strength can strongly perturb the plasmonic band gap properties. We chose this approach to tune the resonance wavelength rather than changing the periodicities of the grating components. Different templates having various exposure times during interference lithography stage, hence with different strengths, were prepared. The reflection spectra of these templates were shown in Fig. 6(a). We observed a shift of the reflection resonance as a function of the grating strength by about 100 nm allowing the tuning of plasmonic resonance through the Stokes shifted Raman lines of the compound under study. SERS measurements were performed by following the same procedure described before and SERS spectra were shown in Fig. 6(b). When the resonance wavelength is close to the Stokes signal, higher enhancement values were calculated. Minimum enhancement occurs when the resonance absorption is close to the laser line. At first glance, this response looks different than previously reported behavior for the case of nano-particles [12]. When metallic nanoparticles used as SERS substrate, maximum SERS enhancement is obtained when plasmonic resonance absorption lies between laser line and Raman emission wavelengths. However, in our case, enhancement caused by the localized field is not as high as it occurs at the near field of the metallic nanoparticles. On biharmonic plasmonic templates, plasmon coupled enhancement mechanism is a dominant factor than the field enhancement factor as observed in this study.

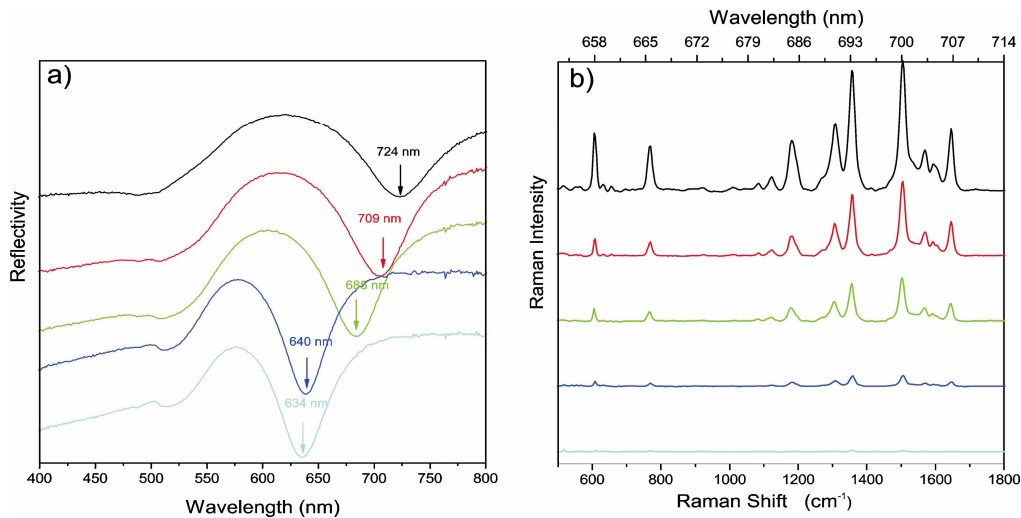


Fig. 6. (a) Resonance absorption spectra of biharmonic metallic gratings with different grating strength. (b) Corresponding SERS spectra for each resonance conditions (Background subtracted and spectra are all shifted for a better view).

4. Enhancement of photoluminescence

In addition to the SPP coupled emission enhancement on the biharmonic grating study, photoluminescence measurements were also performed. As prepared biharmonic metallic surfaces were deposited with a 20 nm thick silicon rich silicon nitride film. Due to the formation of silicon clusters, as deposited silicon nitride has a broad emission spectrum ranging from 500 nm to 800 nm. Experiments were performed at room temperature using Ar^+ laser operating at 488 nm wavelength. Samples were illuminated with the laser and emission was collected in the backscattering configuration and analyzed using a 1-m double spectrometer equipped with photon counting electronics. The emission spectrum of silicon rich silicon nitride film on a flat silicon substrate and the photoluminescence spectrum obtained on the biharmonic surface are shown in Fig. 7 as brown and green curves, respectively. The reflection spectrum of the biharmonic surface (red curve) is also superimposed on Fig. 7 to display the contrast with the photoluminescence enhancement. Figure 7 clearly shows the correlation between plasmonic absorption and enhancement in directional emission of photoluminescence. Photoluminescence spectrum mimics the features of the reflection spectrum both in wavelength and the width of the peaks. The enhancement mechanism is based on the excitation of SPPs on the metal surface [29-31]. Emitted photon couples to the SPPs through higher grating components ($\Lambda_1=500$ nm) or near field effects. We note that, due to the second harmonic component ($\Lambda_2=250$ nm) a plasmonic band gap is formed and SPP density of states (DOS) are increased in the vicinity of the band edges (Fig. 4(a)). Flat dispersion profile around band edges increases the DOS and leads to effective energy transfer [32, 33]. Excited SPPs then scatter into photon states through the grating. It can be calculated from Fig. 7 that biharmonic grating can have directional enhancement by a factor of 30.

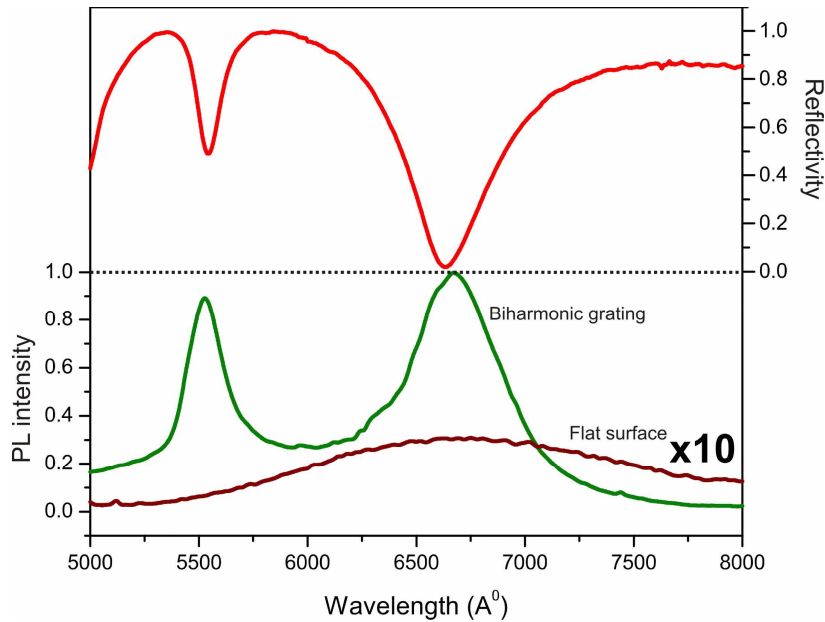


Fig. 7. Normal incidence PL spectrum of biharmonic metallic grating coated with silicon rich silicon nitride. Red curve represents the plasmonic absorption and green curve shows the PL spectrum. There is 30 times enhancement in PL signal at wavelengths coinciding with the plasmonic resonance wavelengths. Brown curve indicates 10 times magnified broad band emission spectrum of silicon rich silicon nitride film on the flat Si surface.

5. Conclusion

We have shown that biharmonic gratings can be used as templates for SERS and photoluminescence enhancement. Due to the plasmonic band gap formation, biharmonic grating surfaces, improve the SPP excitation at the vicinity of the band edges and reveal SERS enhancement factors up to 10^5 . The gratings are stable in air and water at ambient temperatures. The adsorption of analytes is reversible, such that the substrates can be used many times. Such features complement the tunable SERS properties of biharmonic gratings and enhance their potential value for routine chemical and biological sensing. Finally, we showed that grating strengths can be used to tune the plasmonic resonance to optimize the enhancement in Raman signal. We have demonstrated that SPP coupled enhancement is the dominant physical mechanism in our templates.

Acknowledgments

The authors gratefully acknowledge the financial support of Turkish Scientific and Technical Research Council (TUBITAK), grant no: 104M421 and 106T104, UNAM for the use of the ellipsometer and AFM facilities.